European Journal of Mechanics / B Fluids 94 (2022) 106–120

Contents lists available at ScienceDirect

European Journal of Mechanics / B Fluids

journal homepage: www.elsevier.com/locate/ejmflu

Theoretical analysis of vorticity in a hairpin vortex in the viscous sublayer of a laminar boundary layer

L.M. Lin [a,*], Y.X. Wu [a,b]

[a] Key Laboratory for Mechanics in Fluid Solid Coupling Systems, Institute of Mechanics, Chinese Academy of Sciences, Beijing 100190, China
[b] School of Engineering Sciences, University of Chinese Academy of Sciences, Beijing 100049, China

ARTICLE INFO

Article history:
Received 13 August 2020
Received in revised form 26 February 2022
Accepted 1 March 2022
Available online 8 March 2022

Keywords:
Hairpin vortex
Laminar boundary layer
Vortex-induced vortex
Vortex dynamics
Sign law

ABSTRACT

Based on the vortex-induced vortex theory, the classic paradigm of Theodorsen's hairpin vortex is used to analyze the disturbed vorticity and its sign relationship. The hairpin vortex is assumed to exist in the viscous sublayer of a laminar boundary layer, i.e. , the immediate neighborhood of the solid walls. Accordingly, the theoretical model is established mainly by ignoring the inertial forces. The disturbed vorticity field and associated two vorticity sign laws are obtained. The first sign law reveals that the wall-normal vorticity is actually induced by the streamwise vorticity in the two legs, as a kind of interaction between the vortex and solid wall. Such induction is completely a result of the viscous forces, identified as the third viscous effect. Both vorticity sign laws illustrate that the direction of a vorticity vector in the present hairpin vortex is specific, as is the inclined direction of the two legs. Furthermore, the intrinsic relationship between the hairpin vortex and other three-dimensional vortices appearing in external and internal flows at low and laminar Reynolds numbers is thus established by both sign laws. Then, the generalized Π-type vortex is defined as a category of a vortex in which the three vorticity components are consistent with both sign laws through quadrant analysis. In addition, it is theoretically confirmed that the lifting process of the hairpin vortex is predominantly attributable to the mechanism of the vortex-induced vortex and is thus the typical linear process due to viscous forces. Other features, such as the varied inclination, third sign law and self-similarity, are presented in detail.

1. Introduction

Hairpin vortices are very common in various types of laminar–turbulent transitional flows [1], such as the zero-pressure gradient boundary layer of a flat plate at zero incidence, the atmospheric boundary layer over a nearly smooth desert floor, the flow in a smooth-walled pipe and turbulent channel flow. For such a structure of organized motion, the canonical form of nearest-wall flow of concern in this paper is the steady, fully developed and incompressible boundary layer with a zero pressure gradient.

Generally, for flow past a flat plate at zero incidence, the experimental results demonstrating the appearance of hairpin vortices are shown in the basic sketch in Fig. 1, where the Cartesian coordinate system (x, y, z) is established on the plate surface and the x, y and z coordinates are the streamwise, wall-normal (or vertical) and spanwise directions, respectively. The transition in the laminar boundary layer is initially governed by stable laminar flow, the instability of traveling, two-dimensional (2-D) Tollmien–Schlichting (T–S) waves, primary stability theory, and the appearance of unsteady, laminar and three-dimensional (3-D) waves due to secondary instabilities and a characteristic Λ-structure vortex formation [2], as shown in Fig. 1. The 3-D disturbance with increasing T–S instability waves leads to the formation of streamwise vortex pairs in the neighborhood of the laminar boundary layer [3]. This periodic distribution of streamwise vortex pairs along the span further results in the redistribution of the streamwise velocity along the span, forming staggered streaks with high and low speeds in the buffer region [4]. The streaks and the vortices are involved in a self-sustaining nonlinear cycle [5,6]. Meanwhile, the signal of velocity fluctuations is characterized by so-called spikes which denote the appearance of local high shearing regions together with the point of inflection velocity profiles. With increasing disturbance, streamwise vortex pairs around low-speed streaks develop into a horseshoe vortex [7]. The horseshoe vortex is lifted up under self-induction and elongated due to the external shear flow, and thus becomes a hairpin vortex.

Over the past several decades, a large number of experimental and numerical studies have been carried out to investigate the

* Corresponding author.
E-mail address: llmbirthday@163.com (L.M. Lin).

https://doi.org/10.1016/j.euromechflu.2022.03.002
0997-7546/

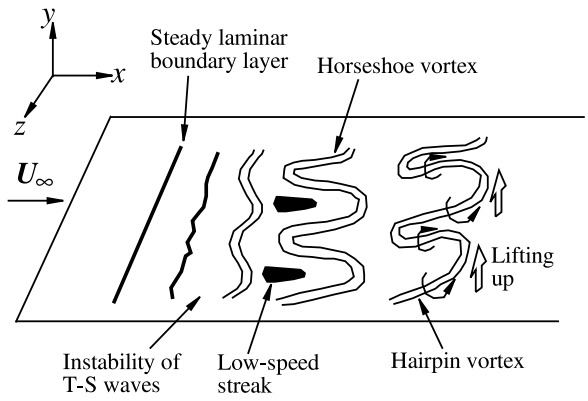

Fig. 1. Diagram of the formation of Tollmien–Schlichting waves and horseshoe and hairpin vortices in the transition of the laminar boundary layer of a flat plate at zero incidence.

dynamics of the structures populating the logarithmic and outer regions of turbulent boundary layers. There are several models for describing the shape of eddies as typical coherent structures [8], which is typically the predominant role of Townsend's attached eddies [9]. The most widespread model is probably the hairpin vortex paradigm, which advocates for attached loop-like vortices or hairpin vortices. Although there is no unique and generally accepted quantitative definition of a hairpin, it is described as a category of vortices consisting of a head (or a negatively rotating arch, thus with the negative spanwise vorticity ω_z) oriented in the spanwise direction and two adjacent legs extending upstream and wall-ward [3]. The classic hairpin (or horseshoe) vortex paradigm was originally proposed by Theodorsen [10], as shown in Fig. 2(a). Such a hairpin vortex can also be generated by introducing the sinuous perturbation of the spanwise velocity [11] and an isolated cuboid roughness and a short duration jet in the boundary layer [12]. Even the hairpin-packet model, described as the streamwise alignment of individual hairpin-like vortices and their hierarchical organization into a coherent packet, is proposed and accounts for the key structural and dynamic characteristics [11,13–15].

In addition to complete hairpin vortices, nonsymmetric incomplete variants (denoted hooks and canes) have also been discovered in many studies [16–18]. At moderate and high Reynolds numbers, it is already reported that the observed, much less organized structures resemble to some extent the clusters [19,20] or small-scale, tube-like structures [21] in turbulent channels and boundary layers. In particular, conditionally averaged structures extracted from the near-wall region of the turbulent boundary layer only show staggered quasistreamwise vortices [22], without a spanwise head-like structure.

Recently, by performing a number of parallel and spatially developing direct numerical simulations on boundary layers, the question of whether hairpin vortices are a dominant feature of near-wall turbulence and which role they play during transition has been investigated in detail [23]. It is found out that secondary hairpin vortices are only created very shortly by nonlinear self-induction after initialization at high Reynolds numbers, including a turbulent viscosity, even with a small amount of the usual background dissipation. Therefore, it is very unlikely that hairpin vortices, as shown in Figs. 2(b) and 2(c) illustrated by different means [23,24], including a forest of hairpins [25], persist in fully developed turbulent boundary layers [22,23,26]. The spatial focus of the form of hairpin vortices is thus placed on the region close to or before the point of the laminar–turbulent transition.

Howbeit, the single hairpin eddy is still a useful paradigm that explains many observations in wall turbulence. Except for the previously discussed experiments and simulations, some theoretical models based on Theodorsen's hairpin vortex paradigm scattered randomly in the streamwise–spanwise plane with a hierarchy of sizes are constructed [27–29]. They are analyzed above the viscous sublayer and mainly in the logarithmic layer. With appropriately chosen parameters for the hairpin geometry and the distribution of the hierarchy, the model reproduces many aspects of statistical quantities such as the mean velocity, Reynolds stresses, and spectra. In particular, the hairpin paradigm provides a mechanism for creating the Reynolds shear stress and low-speed streaks and for transporting the vorticity of the mean shear at the wall away from the wall and for transforming it into a more isotropically distributed small-scale turbulent vorticity, similar to the growth of ramp-shaped hairpin packets or patterns [11,15,30]. In addition, low-speed streaks in the buffer layer also play a crucial role in determining the skin friction and producing turbulent kinetic energy and vorticity because they are the dominant mechanism in the region where most of the change in the mean velocity occurs at low Reynolds numbers [30].

In present vortex dynamics with the conservative body forces, vorticity is only generated on the walls owing to the fluid viscosity. The exception is the small-scale, weak eddies caused by the turbulence, which can be regarded as a kind of background vorticity introduced or randomly distributed in the uniform incoming flow with a certain turbulent intensity. As mentioned above, the hairpin vortex also initially appears and grows in the immediate neighborhood of the walls. Therefore, it is necessary to establish a physical model to describe the hairpin vortex and better understand its dynamic behavior in the viscous sublayer, including the effect on wall turbulence.

In addition, a new physical phenomenon was recently reported through theoretical analysis of the 3-D vorticity field in an external flow past a bluff body [31,32] and an internal flow through a pipe [33] with low and laminar Reynolds numbers. Two universal sign laws for the three components of vorticity were revealed based on the analysis of an introduced vortex or vortex pair in the viscous sublayer of a smooth wall where the viscous forces were dominant. In particular, the mechanism for the generation of the wall-normal vorticity near the wall, which is always equivalent to zero at the wall based on the definition of the vorticity vector, is the so-called vortex-induced vortex, as an indirect effect of the viscous forces. It is believed that such an effect is closely related to the existence of a solid wall [33]. Meanwhile, the theoretical model is mainly established and analyzed in the viscous sublayer as well. Moreover, a recent paper about counterrotating streamwise vortices, such as small-scale turbulent eddies or two legs in a hairpin vortex, introduced in this buffer layer presents a new explanation for the specific sign of the Reynolds shear stress [34]. Therefore, in terms of the sign of the vorticity, it seems that there is a certain intrinsic relationship between the hairpin vortex and other vortices existing in the bluff body's wake or in the secondary flow within a pipe.

In present paper, we try to apply the vortex-induced vortex theory [31] in the basic vortical structure of a single hairpin paradigm in Fig. 2 to investigate the sign relationships among three vorticity components in the viscous sublayer, i.e. , the immediate neighborhood of the solid walls, in a laminar boundary layer. Here, it is not our attempt to rebuild correlated physical relationships that have already been studied and reported in many previous works about the hairpin vortex. However, it is meaningful to explore what kind of correlations the theoretical model constructed in the viscous wall layer can provide or illustrate. First, in Section 2, the physical model is built and analyzed based on different boundary conditions, including vorticity decomposition and some analytical assumptions. Then several features are obtained and discussed in Section 3 in detail. Conclusions are finally offered in Section 4.

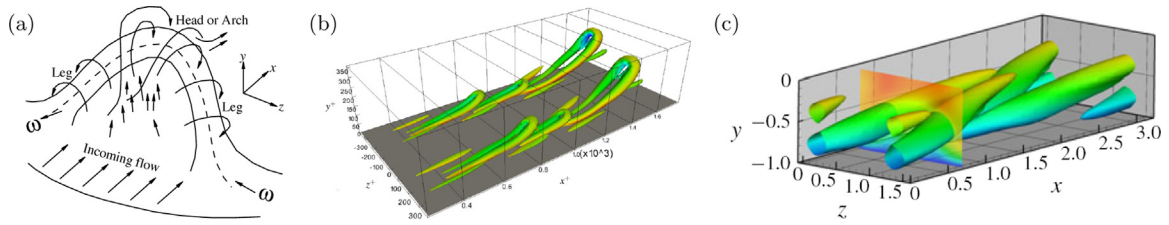

Fig. 2. (a) Theodorsen's conceptualized picture of a hairpin vortex [10]. (b) Isosurfaces of λ_2-criterion showing hairpin-like structures in turbulent boundary layers [23]. (c) Isosurfaces of vortex strength Q illustrating hairpin-like structures in channel flow [24].

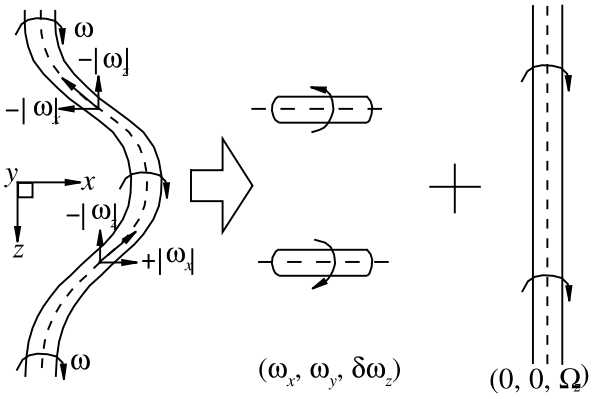

Fig. 3. Schematics of the vorticity field in the hairpin vortex, which is decomposed into the disturbed flow field with the disturbed vorticity $(\omega_x, \omega_y, \delta\omega_z)$ and the mean shear flow with the vorticity $(0, 0, \Omega_z)$.

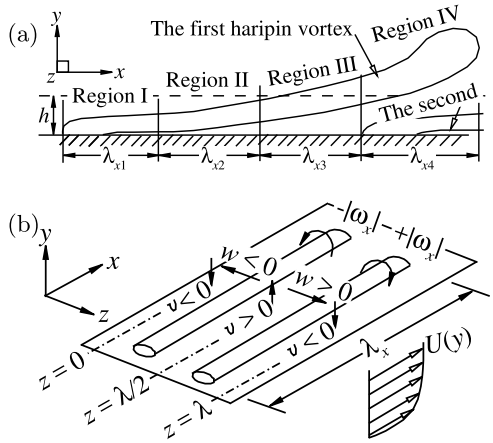

Fig. 4. (a) Different regions in the first hairpin vortex along the streamwise direction. (b) Schematics of streamwise vortex pairs, which are introduced on the boundary layer of a flat plate at zero incidence, and the induced velocity field varied along the spanwise direction, which only exists in a spatial range, $(0 \le x \le \lambda_x, 0 \le y \le h, 0 \le z \le \lambda)$.

2. Physical model

Before establishing a physical model for describing the hairpin vortex, the vorticity field in a single hairpin vortex is decomposed into two parts. In particular, for the whole vorticity field, some assumptions are then proposed or prescribed before presenting subsequent governing equations. Finally, the disturbed vorticity is solved under different boundary conditions in a hairpin vortex.

2.1. Vorticity decomposition in a hairpin vortex

As shown in Fig. 3, the vorticity in the hairpin vortex described by Theodorsen [10] in Fig. 2(a) could be decomposed into two kinds of vorticity fields. One is the disturbed vorticity field with three components of vorticity, $(\omega_x, \omega_y, \delta\omega_z)$, in the local region. The physical mechanism for generating vorticity could be attributed to the result of introducing a geometric disturbance and flow perturbation or of the 3-D instability and turbulence. Here, the physical mechanism is assumed to be the turbulence in the buffer layer. The main feature is the appearance of a single streamwise vortex or counterrotating quasistreamwise vortices. Another is the resultant vorticity in the mean shear flow on the flat plate. Such flow with time-averaged streamwise velocity $U(y)$ is almost two-dimensional with a predominantly spanwise component of vorticity Ω_z. The total spanwise vorticity is then expressed as $\omega_z = \Omega_z + \delta\omega_z$. Then, the total vorticity vector $\boldsymbol{\omega}$ is defined as $(\omega_x, \omega_y, \omega_z)$.

Correspondingly, the total velocity field in the buffer layer can also be decomposed into two parts. One is the disturbed velocity only induced by the disturbed vorticity. Another is the mean shear flow $(U(y), V = 0, W = 0)$ associated with vorticity $\Omega_z(= -\mathrm{d}U/\mathrm{d}y)$.

In addition, in terms of the vortex line, the spanwise waviness of the hairpin vortex mainly results from the local effect of the streamwise vorticity with opposite signs, $\pm|\omega_x|$, on the originally 2-D spanwise vorticity, while the effect of the vertical vorticity, $\pm|\omega_y|$, corresponds to the hairpin vortex tilted upward away from the wall [35].

The disturbed flow field, including the disturbed vorticity $(\omega_x, \omega_y, \delta\omega_z)$ and correlated velocity $\boldsymbol{u} = (u, v, w)$, is thus investigated and analyzed by establishing a theoretical model based on the following assumptions.

2.2. Basic assumptions of the disturbed flow field in a hairpin vortex

On the basis of previous results, as shown in Fig. 2, four regions in the hairpin vortex are classified, as shown in Fig. 4(a):

(1) The first region, Region I, is the initial generation of the hairpin vortex. The counterrotating streamwise vortices or two legs are almost attached on the wall and stretched downstream, as shown in Fig. 2(b). The streamwise length of Region I is λ_{x1}. The streamwise vorticity is much stronger than the vertical vorticity in terms of the vorticity line.

(2) In the second region, Region II, the legs with a concentrated streamwise vorticity are slightly tilted upward away from the wall. The vertical vorticity increases slowly. The streamwise vorticity on the walls decreases but remains nonzero. The streamwise length is λ_{x2}.

(3) When the first hairpin vortex is obviously lifted in Region III, the streamwise vorticity on the wall is almost reduced to zero. The vertical vorticity is obviously increased. The streamwise length is λ_{x3}.

(4) Once the first hairpin vortex is greatly lifted, its head is formed far away from the wall in the fourth region, Region IV. Meanwhile, the streamwise vorticity in the second hairpin vortex could be induced or generated below the first hairpin vortex, as

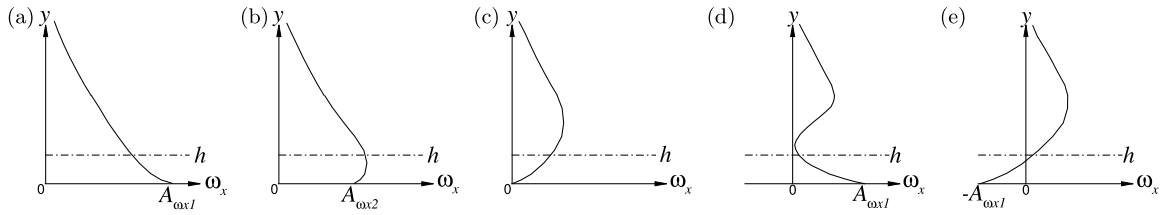

Fig. 5. Estimation of the streamwise vorticity, ω_x, in one leg varied along the vertical distance away from the walls in different regions, (a) Region I, (b) Region II, (c) Region III, (d) Region IV-1, and (e) Region IV-2, where $A_{\omega_{x1}}$ and $A_{\omega_{x2}}$ are amplitudes of ω_x at the walls, and the vertical height h is shown just for illustration.

shown in Figs. 2(b) and 2(c). At the same spanwise position, the sign of the streamwise vortex in the second hairpin vortex may be the same as that in the first hairpin vortex, similar to the case in Fig. 2(b), or opposite to that in the first hairpin vortex corresponding to the case in Fig. 2(c). The streamwise length is λ_{x4}.

The focus is mainly placed on Regions I, II and III within the vertical height h to ensure that the flow analysis is mainly performed in the buffer layer.

Therefore, before presenting the governing equations and boundary conditions in Regions I, II and III, some assumptions and preconditions are presented as follows:

(A1) The inertial coordinate system (x, y, z) is established at the upper surface of the flat plate at zero incidence, as shown in Fig. 4. The x, y and z coordinates are aligned with the streamwise, wall-normal (or vertical) and spanwise directions, respectively. The origin of the coordinates is set to be the start of Region I or II or III on the wall because the disturbed vorticity is naturally convected downstream under the effect of inertial forces.

(A2) The density ρ and viscosity μ of the fluid are constants, as well as the kinematic viscosity $\nu = \mu/\rho$. Thus, the flow is incompressible.

(A3) The local mean shear flow in the boundary layer is fully developed with only the streamwise velocity $U(y)$.

(A4) The body forces are conservative, e.g. , gravity.

(A5) No energy transportation occurs in the present flow.

(A6) A pair of counterrotating streamwise vortices are introduced as the two legs in the boundary layer and evolve downstream, similar to the vortex-induced vortex theory [31]. The streamwise vorticity ω_x is almost uniform along the x-direction and periodically along the z-direction, as shown in Fig. 4(b). The streamwise length scale λ_x is equal to λ_{x1} or λ_{x2} or λ_{x3}, while the spanwise wavelength is λ. They are valid within a specific spatial range, $x \in [0, \lambda_x]$, $y \in [0, h]$ and $z \in [0, \lambda]$. Especially, at the start when $x = 0$ and $y > 0$, it is only possible for ω_x to be nonzero, and $\omega_y = \delta\omega_z = 0$, for simplicity without any qualitative change.

(A7) Three typical boundary cases are analyzed, according to the above Regions I, II and III. As shown in Fig. 5, the streamwise vorticity in one leg that varies along the y-direction is estimated in four different regions. In Region I with $\lambda_x = \lambda_{x1}$, the streamwise vortices are attached on the wall with the maximal vorticity, $|\omega_x|_{y=0} = A_{\omega_{x1}}$, in Fig. 5(a). However, in Region II with $\lambda_x = \lambda_{x2}$, the streamwise vorticity decreases slightly but remains nonzero, $|\omega_x|_{y=0} = A_{\omega_{x2}} (< A_{\omega_{x1}})$, in Fig. 5(b). In Region III with $\lambda_x = \lambda_{x3}$, the streamwise vorticity almost disappears on the wall, i.e. , $\omega_x|_{y=0} = 0$, in Fig. 5(c). In addition, in these typical regions, there is no local recirculation region or reversed flow.

(A8) The inertial forces can be neglected in the immediate neighborhood of the solid walls, i.e. , the viscous sublayer with the vertical height h (equal to 5 viscous lengths). In such a layer, viscous forces are dominant.

2.3. Governing equations of the disturbed flow field

However, in present circumstances, based on the above assumptions (A2–A5, and A8), the nondimensional governing equations for such a disturbed flow field are reduced as:

$$\nabla \cdot \boldsymbol{u} = 0, \tag{1a}$$

$$\nabla p = \frac{1}{Re}\nabla^2 \boldsymbol{u}, \tag{1b}$$

where the symbol ∇ is the gradient operator, $\boldsymbol{u} = (u, v, w)$ is defined as the disturbed velocity vector, p is the disturbed pressure, and Re is the Reynolds number based on the incoming velocity U_∞ $(= U(y \to \infty))$, the characteristic length of flat plate L and kinematic viscosity ν, that is $Re = U_\infty L/\nu$. All velocities are scaled by U_∞ and the lengths are scaled by L.

The non-slip boundary conditions are prescribed at the walls, i.e. , $\boldsymbol{u} = 0$ at $y = 0$. The solutions are only valid in $0 \le x \le \lambda_{x1,2,3}$, $0 \le y \le h$ and $0 \le z \le \lambda$.

Especially, the disturbed pressure is conveniently eliminated from the above governing equations. Then the vorticity transport equation is also reduced as

$$\nabla^2 \boldsymbol{\omega}_\mathrm{d} = 0, \tag{2}$$

where $\boldsymbol{\omega}_\mathrm{d} = (\omega_x, \omega_y, \delta\omega_z)$ is the vector of the disturbed vorticity, defined as $\nabla \times \boldsymbol{u}$.

2.4. Theoretical analysis of the disturbed flow field

Fig. 4(b) shows the schematics of the introduced streamwise vortex pairs with opposite signs on the upper surface of the flat plate. The disturbed velocities, particularly for the vertical and spanwise components v and w, are induced by the introduced streamwise vortices, according to the Biot–Savart law. Based on the above assumption (A6) in each region, their distributions are independent of x and can be assumed as

$$v(y, z) = -A_v(y)\cos(\beta z), \tag{3a}$$

$$w(y, z) = -A_w(y)\sin(\beta z), \tag{3b}$$

where $A_v(y)$ and $A_w(y)$ are amplitudes of v and w, respectively, and $\beta = 2\pi/\lambda$ is the wavenumber. Correspondingly, the boundary conditions for the system of Eq. (1) and under the present assumptions include the absence of slip in the fluid at the walls:

$$A_v|_{y=0} = 0, \tag{4a}$$

$$A_w|_{y=0} = 0. \tag{4b}$$

With the aid of Eq. (3a), the continuity equation, Eq. (1)(a), can be rewritten as

$$\frac{\partial u}{\partial x} = \left(\frac{\mathrm{d}A_v}{\mathrm{d}y} + \beta A_w\right)\cos(\beta z). \tag{5}$$

Because of the non-slip boundary condition on the surface, Eq. (1) gives one limitation for A_v, therefore, given by

$$\left.\frac{\partial v}{\partial y}\right|_{y=0} = 0 \quad \Rightarrow \quad \left.\frac{\mathrm{d}A_v}{\mathrm{d}y}\right|_{y=0} = 0. \tag{6}$$

Then we have:

$$u(x,y,z) = A_u(x,y)\cos(\beta z) + C_u(y,z) = x\left(\frac{dA_v}{dy} + \beta A_w\right)\cos(\beta z) + C_u(y,z), \quad (7)$$

where $A_u(x,y)$ is the amplitude of the disturbed streamwise velocity u, and C_u is an unknown coefficient only related to the coordinates y and z.

The vorticity transport equation, Eq. (2), is adopted for solving the three components of the vorticity defined as

$$\omega_x = \frac{\partial w}{\partial y} - \frac{\partial v}{\partial z} = \left(-\frac{dA_w}{dy} - \beta A_v\right)\sin(\beta z), \quad (8a)$$

$$\omega_y = \frac{\partial u}{\partial z} - \frac{\partial w}{\partial x} = -\beta x\left(\frac{dA_v}{dy} + \beta A_w\right)\sin(\beta z) + \frac{\partial C_u}{\partial z}, \quad (8b)$$

$$\delta\omega_z = \frac{\partial v}{\partial x} - \frac{\partial u}{\partial y} = -x\left(\frac{d^2A_v}{dy^2} + \beta\frac{dA_w}{dy}\right)\cos(\beta z) - \frac{\partial C_u}{\partial y}. \quad (8c)$$

Correspondingly, under the non-slip boundary conditions and assumption (A6), we have $C_u(y,z) = 0$. Hence Eq. (2) reduces to:

$$\left(\frac{d^2}{dy^2} - \beta^2\right)\left(-\frac{dA_w}{dy} - \beta A_v\right) = 0, \quad (9a)$$

$$\left(\frac{d^2}{dy^2} - \beta^2\right)\left(\frac{dA_v}{dy} + \beta A_w\right) = 0, \quad (9b)$$

$$\left(\frac{d^2}{dy^2} - \beta^2\right)\left(\frac{d^2A_v}{dy^2} + \beta\frac{dA_w}{dy}\right) = 0. \quad (9c)$$

It can be seen from Eq. (9a) that the z component is just the space derivative of the y component. The y and z components of disturbed vorticity are interdependent. The physical reason for this is that the continuity of the vorticity satisfies the nondivergence of the vorticity field, i.e. , $\nabla\cdot\boldsymbol{\omega}_d = \frac{\partial\omega_x}{\partial x} + \frac{\partial\omega_y}{\partial y} + \frac{\partial\delta\omega_z}{\partial z} = 0$, where $\partial\omega_x/\partial x = 0$ is assumed in assumption (A6) in each region. Only the x and y components are used to determine the unknown amplitudes A_v and A_w under a certain boundary definition.

2.4.1. The first boundary case in region I

In the present case, in assumption (A7), the streamwise vorticity with a maximal amplitude of $A_{\omega_{x1}}$ (> 0) is attached to the wall, as shown in Fig. 5(a). Thus with the aid of Eqs. (4a)(a) and (8a)(a), we have:

$$|\omega_x|_{y=0} = A_{\omega_{x1}}, \quad \Rightarrow \quad \left.\frac{dA_w}{dy}\right|_{y=0} = A_{\omega_{x1}}. \quad (10)$$

At $y \le h$, the exact solutions of Eq. (9a) can be obtained by the following form:

$$\frac{dA_w}{dy} + \beta A_v = C_1 e^{-\beta y}, \quad (11a)$$

$$\frac{dA_v}{dy} + \beta A_w = C_2\left(e^{\beta y} - e^{-\beta y}\right), \quad (11b)$$

where C_1 and C_2 are positive constants. Finally, the solutions for amplitudes A_v and A_w are given by

$$A_v = \left(\frac{C_2}{2}y - \frac{C_1}{4\beta}\right)\left(e^{\beta y} - e^{-\beta y}\right) + \frac{C_1}{2}ye^{-\beta y}, \quad (12a)$$

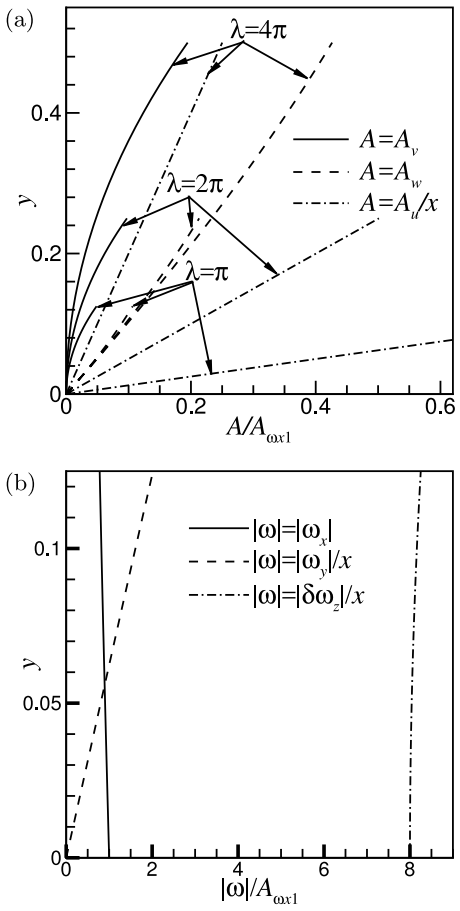

Fig. 6. When $y \le h$, (a) variations in the relative amplitudes, A_v, A_w and A_u divided by $A_{\omega_{x1}}$ in Region I with $C_2 = 2A_{\omega_{x1}}$ with respect to y and λ, and correspondingly, (b) variations in the relative amplitudes of the vorticity, $|\omega_x|/A_{\omega_{x1}}$, $|\omega_y|/(xA_{\omega_{x1}})$ and $|\delta\omega_z|/(xA_{\omega_{x1}})$, along with y at $\lambda = \pi$.

$$A_w = \frac{1}{2\beta}\left(\frac{C_1}{2} + C_2\right)\left(e^{\beta y} - e^{-\beta y}\right) + \frac{C_1}{2}ye^{-\beta y} - \frac{C_2}{2}y\left(e^{\beta y} + e^{-\beta y}\right), \quad (12b)$$

with the following conditions:

$$C_1 = A_{\omega_{x1}}, \quad C_2 \ge 2A_{\omega_{x1}}, \quad h = \frac{C_1}{2\beta C_2}. \quad (13)$$

The distributions of these amplitudes are represented graphically in Fig. 6(a) with the following specific parameters: the constant $C_2 = 2A_{\omega_{x1}}$, the different wavelengths $\lambda = \pi$, 2π and 4π, and therefore the resulting different heights $h_{\lambda=\pi} = 0.125$, $h_{\lambda=2\pi} = 0.25$ and $h_{\lambda=4\pi} = 0.5$. For the sake of the maximum vorticity generated on the wall, the amplitude A_w is obviously greater than the amplitude A_v at the same height. With the increasing wavelength of the disturbance, A_v is reduced at the same height, while A_w varies slightly.

The distributions of the three components of disturbed vorticity are given by

$$\omega_x = -C_1 e^{-\beta y}\sin(\beta z), \quad (14a)$$

$$\omega_y = -C_2\beta x\left(e^{\beta y} - e^{-\beta y}\right)\sin(\beta z), \quad (14b)$$

$$\delta\omega_z = -C_2\beta x\left(e^{\beta y} + e^{-\beta y}\right)\cos(\beta z). \quad (14c)$$

The relative amplitudes of these disturbed vorticity components varying along the vertical position y are shown in Fig. 6(b) with

the example of $\lambda = \pi$. The figure shows that the relative amplitude of $\delta\omega_z$ is obviously larger than that of ω_x or ω_y.

2.4.2. The second boundary case in region II

In the present case, for assumption (A7), the streamwise vorticity with a small amplitude of $A_{\omega_{x2}}$ (> 0 and $< A_{\omega_{x1}}$) at the wall is distributed near the wall, as shown in Fig. 5(b). By similar Eq. (10) but with amplitude $A_{\omega_{x2}}$, we have:

$$\frac{dA_w}{dy} + \beta A_v = C_3 e^{\beta y} + C_4 e^{-\beta y}, \tag{15a}$$

$$\frac{dA_v}{dy} + \beta A_w = C_5 \left(e^{\beta y} - e^{-\beta y}\right), \tag{15b}$$

where C_3, C_4 and C_5 are all positive constants. With the help of the boundary conditions, Eqs. (6) and (4a), the solutions for the amplitudes A_v and A_w are given by

$$A_v = \frac{C_3 - C_4}{4\beta}\left(e^{\beta y} - e^{-\beta y}\right) + \frac{C_5 - C_3}{2} y e^{\beta y} - \frac{C_5 - C_4}{2} y e^{-\beta y}, \tag{16a}$$

$$A_w = \frac{C_3 + C_4 + 2C_5}{4\beta}\left(e^{\beta y} - e^{-\beta y}\right) - \frac{C_5 - C_3}{2} y e^{\beta y} - \frac{C_5 - C_4}{2} y e^{-\beta y}, \tag{16b}$$

with the following conditions:

$$C_3 + C_4 = A_{\omega_{x2}},\ C_4 < C_3 < C_5,\ h < \frac{C_3 + C_4}{\beta(C_5 - C_3)}. \tag{17}$$

The distributions of these amplitudes are represented graphically in Fig. 7(a) with the following specific parameters: the constants are $C_3 = \frac{3}{4}A_{\omega_{x2}}$, $C_4 = \frac{1}{4}A_{\omega_{x2}}$, and $C_5 = A_{\omega_{x2}}$, the different wavelengths are $\lambda = \pi$, 2π and 4π, and therefore the resulting different heights are $h_{\lambda=\pi} \sim 2$, $h_{\lambda=2\pi} \sim 4$ and $h_{\lambda=4\pi} \sim 8$. In the present Region II, the amplitude A_w is still greater than the amplitude A_v at the same height, very close to the walls. With the increasing wavelength of the disturbance, A_v and A_w are both reduced at the same height.

The distributions of the three components of the disturbed vorticity are thus given by

$$\omega_x = -\left(C_3 e^{\beta y} + C_4 e^{-\beta y}\right)\sin(\beta z), \tag{18a}$$

$$\omega_y = -C_5 \beta x \left(e^{\beta y} - e^{-\beta y}\right)\sin(\beta z), \tag{18b}$$

$$\delta\omega_z = -C_5 \beta x \left(e^{\beta y} + e^{-\beta y}\right)\cos(\beta z). \tag{18c}$$

As shown in Fig. 7(b), the relative amplitudes of these three components of the disturbed vorticity all increase as the distance y moves away from the wall.

2.4.3. The third boundary case in region III

In the present case, the vorticity almost disappears at the wall based on assumption (A7), as shown in Fig. 5(c). Such boundary conditions can be expressed on the basis of Eqs. ((4a)a) and ((8a)a) by

$$|\omega_x|_{y=0} = 0, \quad \Rightarrow \quad \left.\frac{dA_w}{dy}\right|_{y=0} = 0. \tag{19}$$

By comparing the boundary condition of A_v from Eq. (6) to the above system in Eq. (9a), it can be concluded that the variations in A_v and A_w are identical. The solutions in $y \le h$ are given by

$$A_v = A_w = A, \tag{20a}$$

$$\frac{dA}{dy} + \beta A = C\left(e^{\beta y} - e^{-\beta y}\right), \tag{20b}$$

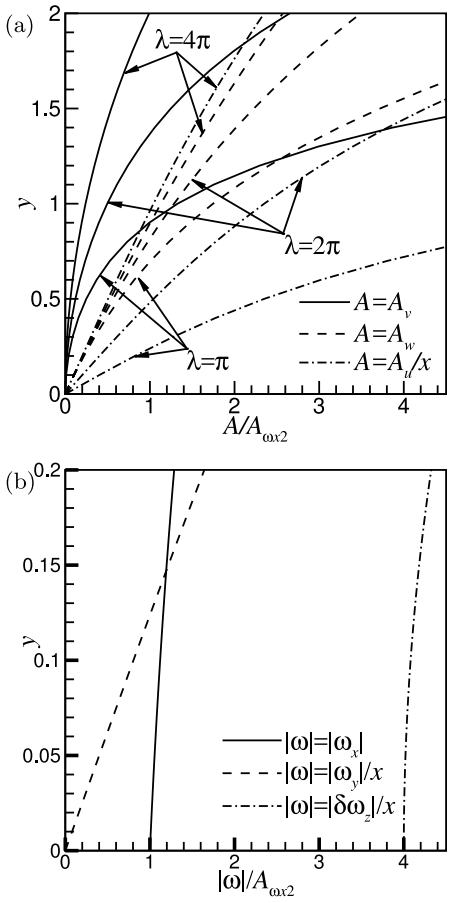

Fig. 7. When $y \le h$, (a) variations in the relative amplitudes, A_v, A_w and A_u divided by $A_{\omega_{x2}}$ in Region II with $C_3 = \frac{3}{4}A_{\omega_{x2}}$, $C_4 = \frac{1}{4}A_{\omega_{x2}}$ and $C_5 = A_{\omega_{x2}}$ with respect to y and λ, and correspondingly, (b) variations in the relative amplitudes of the vorticity, $|\omega_x|/A_{\omega_{x2}}$, $|\omega_y|/(xA_{\omega_{x2}})$ and $|\delta\omega_z|/(xA_{\omega_{x2}})$, along with y at $\lambda = \pi$.

where C is a positive constant. Accordingly, the distributions of the amplitude A near the upper surface are obtained

$$A = \frac{C}{2\beta}\left(e^{\beta y} - e^{-\beta y}\right) - C y e^{-\beta y}, \tag{21}$$

and illustrated in Fig. 8(a) with different wavelengths. With the increasing wavelength, the amplitude would be reduced at the same height.

The disturbed vorticity in the present case is then presented as

$$\omega_x = -C\left(e^{\beta y} - e^{-\beta y}\right)\sin(\beta z), \tag{22a}$$

$$\omega_y = -C\beta x\left(e^{\beta y} - e^{-\beta y}\right)\sin(\beta z), \tag{22b}$$

$$\delta\omega_z = -C\beta x\left(e^{\beta y} + e^{-\beta y}\right)\cos(\beta z). \tag{22c}$$

These amplitude variations are shown in Fig. 8(b) and increase as y increases.

In the present disturbed vorticity field, Eqs. (14a), (18a) and (22a) show that the appearance of ω_y and $\delta\omega_z$ downstream ($x > 0$) is actually induced by the introduced ω_x, which interacts with the walls [33] because ω_y and $\delta\omega_z$ at the start of Regions I, II and III always disappear in assumption (A6), particularly for ω_y owing to $\omega_y(y = 0) \equiv 0$, as stated below in detail. This is the key idea in the vortex-induced vortex theory [31,33].

In addition, the disturbed vertical vorticity ω_y is always proportional to $\beta x\left(e^{\beta y} - e^{-\beta y}\right)$, while $\delta\omega_z$ is proportional to $\beta x\left(e^{\beta y} + e^{-\beta y}\right)$, throughout the present three regions. This means

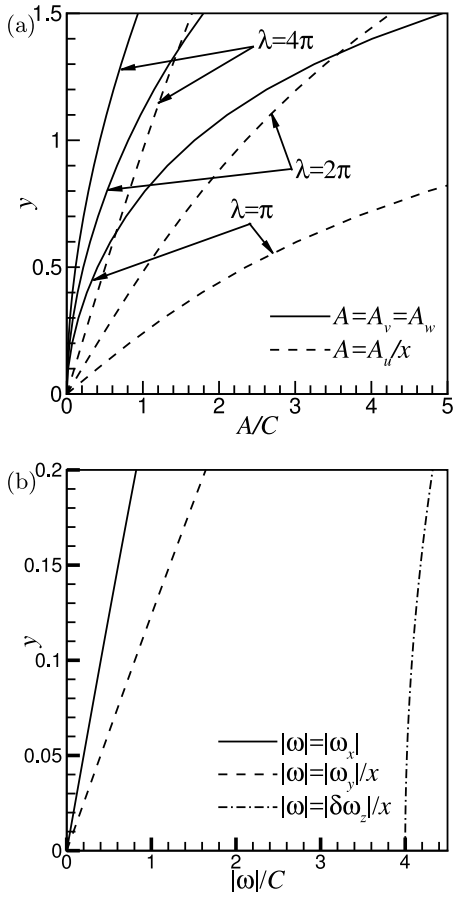

Fig. 8. When $y \leq h$, (a) variations in the relative amplitudes, A_v, A_w and A_u divided by C in Region III with respect to y and λ, and correspondingly, (b) variations in the relative amplitudes of the vorticity, $|\omega_x|/C$, $|\omega_y|/(xC)$ and $|\delta\omega_z|/(xC)$, along with y at $\lambda = \pi$.

that both amplitudes of ω_y and $\delta\omega_z$ would increase with increasing y.

3. Results and discussions

3.1. The first sign law for the disturbed streamwise and vertical vorticities

From the above specific distribution of the streamwise and vertical components of the disturbed vorticity under different circumstances, the first sign law in Regions I, II and III of the hairpin vortex is obtained. Similar to the previous work [31], by introducing the first sign variable $\varpi_1 = \omega_x \cdot \omega_y$, we have

$$\varpi_1 = C_1 C_2 \beta x \mathrm{e}^{-\beta y}\left(\mathrm{e}^{\beta y} - \mathrm{e}^{-\beta y}\right)\sin^2(\beta z), \quad \text{in Region I,} \tag{23a}$$

$$\varpi_1 = C_5 \beta x \left(C_3 \mathrm{e}^{\beta y} + C_4 \mathrm{e}^{-\beta y}\right)\left(\mathrm{e}^{\beta y} - \mathrm{e}^{-\beta y}\right)\sin^2(\beta z), \quad \text{in Region II,} \tag{23b}$$

$$\varpi_1 = C^2 \beta x \left(\mathrm{e}^{\beta y} - \mathrm{e}^{-\beta y}\right)^2 \sin^2(\beta z), \quad \text{in Region III.} \tag{23c}$$

Or we can rewrite these as follows:

$$\mathrm{sgn}(\varpi_1) = 1, \tag{24}$$

except for some special positions where $\varpi_1 = 0$ ($z = 0$, $\frac{1}{2}\lambda$ and λ), where the sign function $\mathrm{sgn}(f)$ with nonzero f is stated as

$$\mathrm{sgn}(f) = \begin{cases} 1 & \text{if } f > 0, \\ -1 & \text{if } f < 0. \end{cases} \tag{25}$$

The first sign law is unaffected by the sign of the (disturbed) spanwise vorticity $\delta\omega_z$ or Ω_z and unrelated to the Reynolds number Re and wavelength λ or wavenumber β.

The physical mechanism responsible for the generation of the disturbed vertical vorticity ω_y with specific signs in the hairpin vortex is revealed. At first, the disturbed vertical vorticity always disappears at the walls, as expressed by Eq. (8a)(b) with a nonslip velocity $u = w = 0$ at $y = 0$. Only the streamwise and spanwise components of the disturbed vorticity, ω_x and $\delta\omega_z$ in Eq. (8a), are generated and associated with the disturbed shear flow near the walls, such as $\partial w/\partial y \neq 0$ and $\partial u/\partial y \neq 0$ at the walls in Region I. The first sign law then indicates that in Fig. 3 or 4, $+|\omega_y|$ is induced by introducing $+|\omega_x|$ in one leg at $z = \frac{3}{4}\lambda$, while $-|\omega_y|$ is induced by $-|\omega_x|$ in another leg at $z = \frac{1}{4}\lambda$. In other words, the wall-normal vorticity near the walls is actually induced by one of the wall-tangent vorticities at the walls, from the viewpoint of the vorticity generation. These specific signs of ω_y are theoretically determined by the spanwise distribution of u, i.e. , $\partial u/\partial z$ in Eq. (8a)(b) (see in Section 3.4. Even if the legs of the hairpin vortex are tilted upward away from the walls in both Regions II and III, where the streamwise vorticity begins to decrease to zero at the walls, the vertical vorticity with a specific sign is still induced by the counterrotating streamwise vortices, advected or evolved from those in Region I, under the same mechanism of the first sign law. These special distributions of ω_x and induced ω_y are well consistent with the spacial development of the vortex lines in the hairpin vortex [11,35]. Therefore, the first sign law is valid in the whole hairpin structure.

3.2. The second sign law for the three components of vorticity

First, the 2-D mean shear flow past a flat plate without any flow or geometry disturbance is described. There is only spanwise vorticity Ω_z attached at the walls and convected upward away from the walls. Such mean shear flow is dominated by the streamwise velocity $U(y)$. In the viscous sublayer, $U(y)$ is linear, i.e. , $U(y) = \eta y$, where η is a positive coefficient related to the friction velocity at the wall. As a result, the vorticity Ω_z is mainly determined by $-\mathrm{d}U/\mathrm{d}y$, i.e. , $\Omega_z = -\eta$. The sign of Ω_z is thus negative in the whole of Regions I, II and III and is simply expressed by

$$\mathrm{sgn}(\Omega_z) = -1. \tag{26}$$

Then, the effect of the disturbed spanwise vorticity $\delta\omega_z$ can be obtained. It is assumed that the magnitude of the disturbed spanwise vorticity $|\delta\omega_z|$ is less than that of $|\Omega_z|$ in the mean shear flow, i.e. , $|\delta\omega_z| < |\Omega_z|$, in Regions I, II and III. It is expressed as $\mathrm{sgn}(\Omega_z + \delta\omega_z) = \mathrm{sgn}(\omega_z) = -1$. Then, the variation in $\delta\omega_z$ does not have a significant influence on the qualitative distribution of Ω_z. Subsequently, the appearance of $\delta\omega_z$ can be regarded as the wavy modification of Ω_z, similarly for $u(x, y, z)$ to $U(y)$. For example, in Region I in the viscous sublayer, we have

$$U + u = \eta y + C_2 x\left(\mathrm{e}^{\beta y} - \mathrm{e}^{-\beta y}\right)\cos(\beta z), \tag{27a}$$

$$\Omega_z + \delta\omega_z = -\eta - C_2 \beta x\left(\mathrm{e}^{\beta y} + \mathrm{e}^{-\beta y}\right)\cos(\beta z). \tag{27b}$$

In the present situation, as indicated by Eq. (14a)(c), or (18a)(c), or (22a)(c), $\delta\omega_z$ is negative near $z = 0$ or λ (the start of the leg) but positive near $z = \lambda/2$ (the head). Meanwhile, as the wall-normal distance increases, the amplitude of the disturbed vorticity $\delta\omega_z$ increases, but the amplitude of Ω_z decreases gradually over the

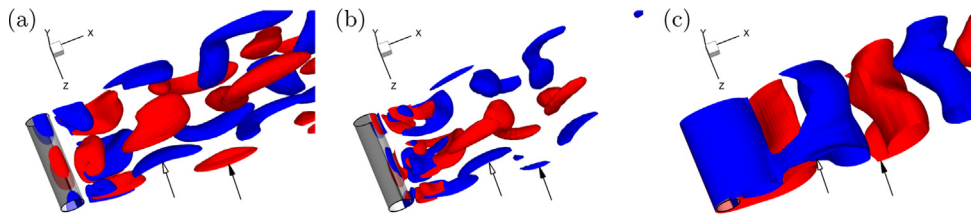

Fig. 9. Pure mode A illustrated by the isosurfaces of (a) $\omega_x = \pm 0.3$, (b) $\omega_y = \pm 0.3$ and (c) $\omega_z = \pm 0.3$ in the wake of a circular cylinder at $t = 872$ and $Re = 200$, where red and blue colors denote positive and negative values, respectively, and the arrows with the hollow and filled heads denote the vorticity with the specific sign originally formed in the upper and lower shear layers, respectively. Note that the cylinder surface is denoted by the gray semi-translucent surface. (For interpretation of the references to color in this figure legend, the reader is referred to the web version of this article.)

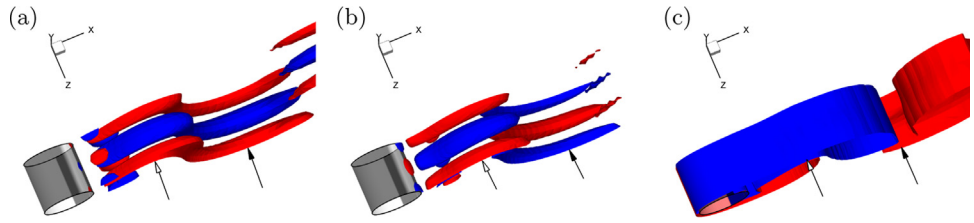

Fig. 10. Pure mode B illustrated by the isosurfaces of (a) $\omega_x = \pm 0.2$, (b) $\omega_y = \pm 0.2$ and (c) $\omega_z = \pm 0.2$ in the wake of a circular cylinder at $t = 931.5$ and $Re = 300$, where red and blue colors denote positive and negative values, respectively, and the arrows with the hollow and filled heads denote the vorticity with the specific sign originally formed in the upper and lower shear layers, respectively. Note that the cylinder surface is denoted by the gray semi-translucent surface. (For interpretation of the references to color in this figure legend, the reader is referred to the web version of this article.)

viscous sublayer. Consequently, these coupled effects result in the increase in the strength of the total spanwise vorticity ω_z $(= \Omega_z + \delta\omega_z)$ at the start of the leg and lower vertical position but the strength decreases greatly at the head of the hairpin vortex and higher vertical position in Fig. 3. If the magnitudes of ω_x and ω_y in the (x, y)-plane of the two legs are approximately equivalent to the reduced magnitude of ω_z in the head, then the isosurface of ω can represent the two legs and the head of the hairpin vortices, e.g. , in Fig. 2(b). However, the start of the legs near $z = 0$ and λ or the region between the two adjacent hairpin vortices along the z-axis is hard to show in the isosurface of ω because ω_z is significantly larger than ω_x and ω_y (≈ 0) at the lower vertical positions.

Based on the above analysis, by introducing the second sign variable $\varpi_2 = \omega_x \cdot \omega_y \cdot \omega_z$ [31], the second sign law for the three components of the vorticity is then obtained as

$$\mathrm{sgn}(\varpi_2) = -1, \tag{28}$$

except for at certain positions where $\varpi_2 = 0$ ($z = 0$, $\frac{1}{2}\lambda$ and λ). It can be seen that such a sign relationship is also independent of Re, λ and β in Regions I, II and III.

3.3. Intrinsic relationship with 3-D vortices in external and internal flows at low and laminar Reynolds numbers

Let us briefly review some features in 3-D vortex-shedding patterns that appear in external flow (EF) past a bluff body at low, laminar Reynolds numbers. The 3-D laminar wake transition of a circular-section cylinder, caused by 3-D instability, is first presented [32,36]. Two sign laws for dominant vorticities in (pure) modes A and B, typically as shown by the arrows with the hollow and filled arrowheads in Figs. 9 and 10 through direct numerical simulations, are summarized in the near wakes at Reynolds numbers of 200 and 300, respectively. Among them, the first sign law is thus expressed as follows:

$$\mathrm{sgn}(\varpi_1) = \begin{cases} -1, & \text{if } y < 0, \\ 1, & \text{if } y > 0, \end{cases} \tag{29}$$

where regions at $y > 0$ and $y < 0$ denote the upper and lower shear layers, respectively, and the spanwise vortices (including concentrated vortex cores and elongated and stretched braids) are shed from the upper and lower shear layers, respectively. The second sign law is exactly the same as that in Eq. (28). These features are also found in the 3-D laminar wake transition of a square-section cylinder for (pure) modes A and B at $Re = 180$ and 250 [37,38], respectively.

Different from the above 3-D instability, some kinds of geometric disturbances introduced in the straight circular- and square-section cylinders can also result in the appearance of 3-D vortex-shedding patterns at low Reynolds numbers [37,39,40]. For example, in the wake of a square-section cylinder with a wavy stagnation face at $Re = 100$, such wavy disturbances at a certain intensity lead to the appearance of a hairpin-like or Ω-like vortex in the near wake, the complete suppression of Kármán vortices and both the upper and bottom shear layers extending downstream [37,39]. Moreover, these 3-D vortex-shedding patterns also exist in the wake of a circular-section cylinder with radial disturbances [40]. Interestingly, similar sign laws for dominant vorticity components are summarized through careful comparisons [32]. In particular, the two sign laws (in the downstream region $x > 0$) are exactly the same as those in Eqs. (28) and (29), typically as shown in Fig. 11 when Kármán vortices are totally suppressed in the near wake [31].

Recently, through theoretical analysis of the secondary flow within a circular-section pipe as typical internal flow (IF) at low and laminar Reynolds numbers, two sign laws for the disturbed vorticity in the cylindrical coordinate system (z, r, ϕ) are determined [33], where the z, r and ϕ coordinates are the axial, radial and azimuthal directions, respectively. If the curved wall reaches a flat plate when the radius R approaches infinity and the local Cartesian coordinate system is adopted at the wall, then both sign laws at the downstream regions ($z > 0$ in IF) are exactly the same as those in the upper surface of the flat plate, i.e. , Eqs. (24) and (28). This indicates that vorticity sign laws are universal, regardless of the EF and IF, or coordinate systems. For convenience, the following analysis is mainly conducted in the downstream region of EF ($x > 0$), including the upper and lower plate surfaces and both sides of a bluff body's wake with and without geometric disturbances.

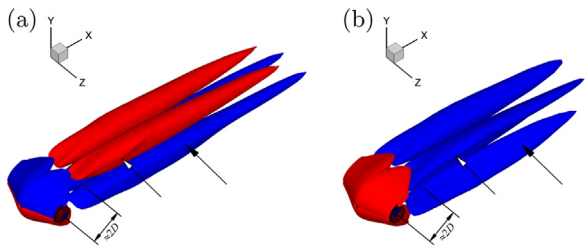

Fig. 11. In a case of Kármán vortices completely suppressed in the wake of a conic cylinder where the radius varies across the span in the Λ form, both sign laws illustrated by the isosurfaces of the first and second sign variables, (a) $\varpi_1 = \pm 0.04$ and (b) $\varpi_2 = \pm 0.03$ at $t = 230$, non-dimensional wavelength of 4, dimensionless wave height of 0.8 and $Re = 100$, where red and blue colors denote positive and negative values, respectively, and the arrows with the hollow and filled heads denote ϖ_1 and ϖ_2 with the specific sign originally formed in the upper and lower shear layers, respectively. Note that the cylinder is denoted by the gray translucent surface.

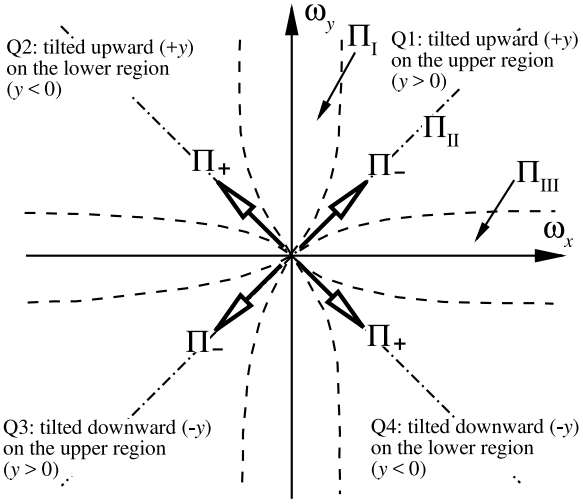

Fig. 12. Quadrant analysis of the local streamwise and vertical components of the vorticity, (ω_x, ω_y), for different types of 3-D vortices tilted upward $(+y)$ or downward $(-y)$ in the (x, y)-plane, according to both sign laws in Eqs. (28) and (29), where the dash-dot lines denote $|\omega_x| = |\omega_y|$, and the dashed lines are used to qualitatively separate the different vortex patterns according to the relative strength or the ratio of ω_y to ω_x, and the hollow arrows denote the inclined direction of vortex lines determined by ω_x and ω_y in the (x, y)-plane.

Then, the specific vorticity signs in the above vortical structures can be clarified as follows. Based on the above two sign laws for the vorticity in a hairpin vortex, we can determine the specific group of the vorticity signs. For example, $(+|\omega_x|, +|\omega_y|, -|\omega_z|)$ exists in one leg tilted upward, while $(-|\omega_x|, -|\omega_y|, -|\omega_z|)$ appears in another leg tilted downward, as shown in Fig. 2(a). They are exactly the same as those existing in the vortices in pure modes A and B in wakes of circular- and square-section cylinders [32,36,38], i.e. , the so-called Π_- vortex formed in the upper shear layer and shed in the upper side of the wake. In addition, there is another kind of vortex that has a different group of vorticity signs, that is, $(+|\omega_x|, -|\omega_y|, +|\omega_z|)$ and $(-|\omega_x|, +|\omega_y|, +|\omega_z|)$. Such a vortex is referred to as the Π_+ vortex formed in the lower shear layer and shed in the lower side of the wake, therefore satisfying the relationship in Eq. (29) in region $y < 0$ and Eq. (28). For such a Π-type vortex itself, the head line, '—', denotes the spanwise vortex alternately shed from the upper or lower shear layer. While two legs, '| |', denote that streamwise and/or vertical vortex pairs with opposite signs are also alternatively shed and stretched or elongated by the upstream spanwise vortex. Therefore, a conclusion can be made that the hairpin vortex formed in the lower flat plate $(y < 0)$ has the same group of vorticity signs in the Π_+ vortex. Consequently, in terms of the vorticity sign, the hairpin vortex is very similar to a Π-type vortex but with a smaller scale, schematically illustrated in the right part of the vorticity decomposition in Fig. 3.

In summary, the intrinsic relationship between the hairpin vortex and vortices in EF and IF has two aspects: two vorticity sign laws and specific sign combinations among the three vorticity components. This results in a qualitative similarity among these vortices. It may be conjectured that both the sign laws and sign similarity in these different vortical structures discussed here are also the universal physical mechanism, suggested in a previous paper [41], for a number of wall-bounded shear flows including the boundary layers, channel and pipe flows, transitional and turbulent flows, and for different vortices, such as the appearance of a vortex loop, formation of the Λ- or hairpin-vortex, and the hairpin-V-hairpin structure induced by an isolated cuboid roughness coupled with a short duration jet [12], even a train of Ω- and ring-like vortices. Particularly in a recent work [42], it is reported that such hairpin-like vortex also appears in a supersonic, separated and longitudinal cylinder wake. This similarity could be attributed to the fact that both sign laws are unrelated to the Reynolds number, the wavelength of the disturbances introduced artificially (geometrical disturbance) or naturally (roughness, 3-D instability and turbulence), and the solid structures in EF and IF. Such a conjecture may establish a new, universal theory of vorticity-sign similarity in vortices determined by present vortex dynamics, although much more evidence is needed in experiments and direct numerical simulations.

In addition, as shown in Fig. 12, a quadrant analysis for the streamwise and vertical components of the vorticity is performed. As stated above, the Π_- vortex mainly appears in the first (Q1) and third (Q3) quadrants of the $\omega_x - \omega_y$ plane, while the Π_+ vortex exists in the second (Q2) and fourth (Q4) quadrants. Hence, we can define the generalized Π-type vortex as a category of a specific vortex in which three components of the dominant vorticity satisfy both sign laws, regardless of EF or IF and even in the boundary layer. Furthermore, according to the relative strength, i.e. , the ratio of ω_y to ω_x, in vortical structures, different vortices can be classified into three categories, typically in Q1, as shown in Fig. 12. In the first category of the Π-type vortex, $\Pi_{\rm I}$, the vertical vorticity ω_y is obviously greater than the streamwise vorticity ω_x, e.g. , $|\omega_y/\omega_x| > 2 \sim 5$. The typical case is the totally suppressed Kármán vortices in the wakes of a wavy square-section cylinder and a conic cylinder [37,40], as shown in Fig. 11. The second category, $\Pi_{\rm II}$, is denoted by the equivalent magnitudes between ω_x and ω_y. It includes many kinds of vortices, typical (pure) modes A and B in the bluff body's wakes [36,38] in Figs. 9 and 10, the head of the hairpin vortex, and the head of the Ω-like vortex shedding in the wake of the geometrically disturbed cylinders [32,37]. For the third category of the Π-type vortex, $\Pi_{\rm III}$, the magnitude of the vertical vorticity is less than that of the streamwise vorticity, e.g. , $|\omega_y/\omega_x| < 0.1$, typically in the horseshoe vortex, quasistreamwise vortices, two legs of the hairpin vortex, and legs of the Ω-like vortex in the disturbed cylinder's wake.

3.4. Disturbed velocity and pressure fields

Except for the vertical and spanwise components of the disturbed velocity, v and w, which are assumed to be uniform along the x direction in each region (I, II or III), the main focus is on the backward induced flow u and pressure p distributed in the nearest wall.

In the present analysis model and in Regions I, II and III, the disturbed streamwise velocity u is obtained as follows:

$$u(x, y, z) = C_2 x \left(e^{\beta y} - e^{-\beta y}\right) \cos(\beta z)$$

$$\text{in Region I,} \tag{30a}$$

$$u(x,y,z) = C_5 x\left(e^{\beta y} - e^{-\beta y}\right)\cos(\beta z)$$

$$\text{in Region II,} \tag{30b}$$

$$u(x,y,z) = Cx\left(e^{\beta y} - e^{-\beta y}\right)\cos(\beta z)$$

$$\text{in Region III.} \tag{30c}$$

Their amplitudes are shown in Figs. 6(a), 7(a) and 8(a). Particularly, the low-speed streaks always appear in the middle region, $z \in (\frac{1}{4}\lambda, \frac{3}{4}\lambda)$, because $u < 0$, while the high-speed region with $u > 0$ exists outside of the two legs or between the legs of the adjacent hairpin vortices, $z < \frac{1}{4}\lambda$ or $z > \frac{3}{4}\lambda$. In addition, the backward induced velocity u is always proportional to $x\left(e^{\beta y} - e^{-\beta y}\right) \approx 2\beta xy$ when $y \to 0$, regardless of Region I, II or III. It also shows that the larger the hairpin vortex with the larger wavelength λ or lower wavenumber β is, the weaker the backward induced flow u is, owing to the greater mean distance from the vortex elements in the hairpin core to the center of the hairpin loop, consistent with the previous description [30]. Meanwhile, such a streamwise velocity u induced by the quasistreamwise vortices mainly determines not only the wall-normal vorticity ω_y $(= \partial u/\partial z)$, as stated in Section 3.1, but also another wall-tangent vorticity $\delta\omega_z$ $(= -\partial u/\partial y)$.

Meanwhile, the disturbed pressure p is presented as

$$p(y,z) = -\frac{C_2}{Re}\left(e^{\beta y} - e^{-\beta y}\right)\cos(\beta z) - \frac{C_1}{Re}e^{-\beta y}\cos(\beta z) + C_{p1} \quad \text{in Region I,} \tag{31a}$$

$$p(y,z) = \frac{1}{Re}\left[-(C_5 - C_3)e^{\beta y} + (C_5 - C_4)e^{-\beta y}\right]\cos(\beta z) + C_{p2} \quad \text{in Region II,} \tag{31b}$$

$$p(y,z) = \frac{2C}{Re}e^{-\beta y}\cos(\beta z) + C_{p3} \quad \text{in Region III,} \tag{31c}$$

where C_{p1}, C_{p2} and C_{p3} are constants. Considering the analysis in Section 3.9, such pressure could be regarded as the variation in the pressure in each region (I, II or III). Therefore, there are two relationships for the varied pressure on the wall ($y = 0$):

(i) In the middle region of the hairpin vortex ($z \sim \frac{1}{2}\lambda$), $p - C_{p1} = C_1/Re > 0$ in Region I, $p - C_{p2} = (C_4 - C_3)/Re < 0$ in Region II and $p - C_{p3} = -2C/Re < 0$ in Region III, which means that the pressure would decrease downstream, and the local reversed flow with a total velocity of $U + u < 0$ could occur;

(ii) In the outboard region of the hairpin vortex ($z \sim 0$ or λ), $p - C_{p1} < 0$ in Region I, $p - C_{p2} > 0$ in Region II and $p - C_{p3} > 0$ in Region III, which indicates that the pressure would increase along the streamwise direction.

It should be noted that the pressure used in the present dynamics, Eq. (1)(b), is only affected or determined by the viscous forces, totally unrelated to the inertial forces. Such pressure variation is actually the so-called frictional pressure loss. Consequently, it can be concluded that the favorable pressure gradient is in the outboard region, and the adverse pressure gradient is in the middle region, if the pressure variation owing to the inertial forces, i.e. , kinetic pressure, is taken into account.

3.5. The third sign law and sign of the Reynolds shear stress

Except for the above two sign laws for the vorticity, there is a third sign law for the two disturbed velocity components, u and v, induced by the introduced streamwise vortex. Based on Eqs. (7), (30a) and ((3a)a), we have the following relationship:

$$uv = -xA_v\left(\frac{dA_v}{dy} + \beta A_w\right)\cos^2(\beta z) \le 0. \tag{32}$$

Or it can be rewritten by introducing the third sign variable $\varpi_3 = u \cdot v$ [31] as

$$\text{sgn}(\varpi_3) = -1, \tag{33}$$

except for some specific positions where $\varpi_3 = 0$ ($z = \frac{1}{4}\lambda$ and $\frac{3}{4}\lambda$). It is also unrelated to Regions I, II and III, the Reynolds number and wavelength.

Such a relationship is predicted in the turbulent boundary layer of the flat plate [34] and has already been reported in previous work [31]. In the turbulent boundary layer, the introduced streamwise vortex (with one leg) or vortex pair (with two legs) results from turbulence in the local region or is viewed as small-scale eddies. The disturbed velocity $\boldsymbol{u}$ is then induced by such a streamwise vortex and is different from the mean shear flow $(U, 0, 0)$. Thus, $\boldsymbol{u}$ can be viewed as the turbulence-induced velocity. The Reynolds stress is defined as $-\rho uv$. In the present circumstance, we first have $-\rho uv = -\rho\varpi_3 \ge 0$ in Region I or the laminar sublayer where the viscous forces are dominant. When the quasistreamwise vortices or counterrotating vortex pairs, as well as the horseshoe or hairpin vortex, evolve or advect in Regions II and III, the Reynolds stress is still positive based on the third sign law. Finally, the whole viscous sublayer is full of vortices with positive shearing stresses. Therefore, the above process develops the hypothesis that the positive Reynolds shear stress is inherently accompanied by a quasistreamwise vortex or vortex pairs generated and evolved in the turbulent boundary layer, as proposed in the previous work [34]. It should be mentioned that the existence of the head or formation of the complete hairpin vortex is not a necessary condition in this process.

Moreover, as shown in Figs. 6(a), 7(a) and 8(a), the amplitude relationship among the three components of disturbed velocity is obtained as follows,

$$A_u > A_w \ge A_v. \tag{34}$$

This is true in most cases ($x > h$ in Region I, $x > \frac{C_3+C_4}{2\beta C_5}$ in Region II, $x > 0$ in Region III), as verified in previous work [34] mainly in Region I, through the comparing ratios A_w/A_u and A_v/A_w in different regions and $y \to 0$.

3.6. New interpretation of the lifting-up hairpin vortex

In this subsection, a new lifting mechanism is proposed on the basis of present theoretical models for the hairpin vortex. First, different mechanisms for the lifting-up hairpin vortex are reviewed briefly. Then, the ratio of ω_y to ω_x predicted by the present theoretical model is illustrated. Subsequently, the effect of ejections on the lifting mechanism is discussed from different aspects in detail. Finally, the new mechanism based on the vortex-induced vortex theory is used to explain the lifting-up phenomenon.

3.6.1. Brief review

There are at least two mechanisms used to explain the lifting of the hairpin vortex reported in previous works. First, in the Theodorsen's conceptual model of the hairpin vortex, as shown in Fig. 2(a), Theodorsen visualized a vortex filament oriented spanwise to the mean flow and perturbed by a small upward motion [10]. The part of the filament lying further away from the wall (variously called the head) would experience a higher mean flow velocity and be convected downstream faster than its lower-lying parts. Consequently, the legs connecting the spanwise part of the vortex to the head would be stretched and intensified, causing the vortex to lift away from the wall at a higher mean velocity, resulting in greater stretching compared to that the lower-lying parts.

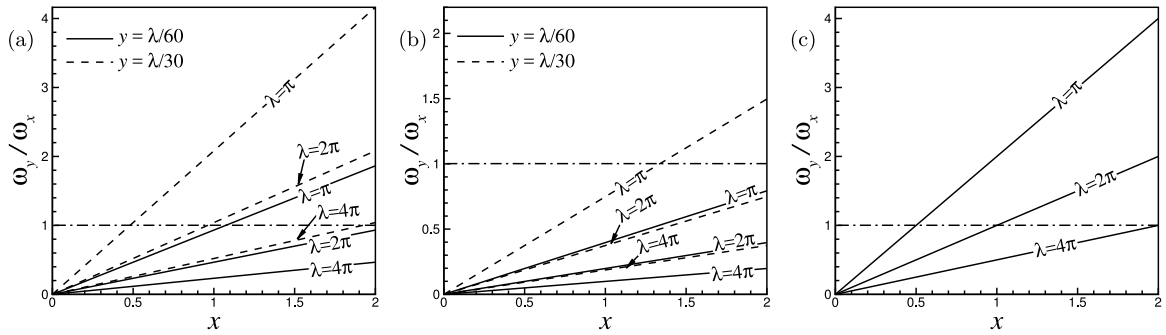

Fig. 13. The ratio ω_y/ω_x varying along the x-direction in (a) Region I, (b) Region II and (c) Region III with different wavelengths, where C_2 is assumed to be $2C_1$ in subfigure (a), and $C_3 = \frac{3}{4}C_5$ and $C_4 = \frac{1}{4}C_5$ are prescribed in subfigure (b), and dash-dot lines denote $|\omega_y| = |\omega_x|$.

Then, through observations of H_2 bubbles in the $(x-y)$ planes, the bursting model was proposed by Kline et al. [4]. The long streamwise streaks of bubbles were shown to be regions of low streamwise momentum. The low-speed regions were associated with quasistreamwise vortices lifting the viscously retarded fluid upwards from the region close to the wall. The bubble streaks wavered vertically with increasing amplitude and then lifted away from the wall in a vigorous, chaotic motion.

The common and key phenomenon appearing in these two mechanisms is negative streamwise fluctuations (i.e. , $-|u|$) being lifted away from the wall by positive wall-normal fluctuations (i.e. , $+|v|$), referred to as ejections [43]. Such ejections correspond to the lifting process of low-speed fluid that originates near the wall by the present upwelling flow between the two legs of the Λ-like or hairpin-like vortex [35].

3.6.2. Ratio of ω_y/ω_x in the present hairpin vortex model

The characteristics of the slope of the hairpin vortex are analyzed qualitatively. Similar to the discussion for both sign laws mentioned above, from the viewpoint of the spatial evolution of vortex lines, the skewed angle of the vortex lines in the (x, y) plane is mainly determined by the ratio ω_y/ω_x.

From Eqs. (14a), (18a) and (22a), this ratio is obtained in different regions as follows:

$$\frac{\omega_y}{\omega_x} = \frac{C_2}{C_1}\beta x\left(e^{2\beta y}-1\right), \quad \text{in Region I} \tag{35a}$$

$$\frac{\omega_y}{\omega_x} = \frac{C_5\beta x\left(e^{2\beta y}-1\right)}{C_3 e^{2\beta y}+C_4}, \quad \text{in Region II} \tag{35b}$$

$$\frac{\omega_y}{\omega_x} = \beta x, \quad \text{in Region III.} \tag{35c}$$

In particular, the ratio ω_y/ω_x in Region III is unrelated to the wall-normal distance y.

As shown in Fig. 13, the variation in this ratio along with streamwise positions at different wavelengths is illustrated in three typical regions. As the wavelength decreases, the ratio increases, which indicates that the small-scale hairpin vortex slants upward quickly. The figure shows that the increasing rate of this ratio along the x-axis at the same wavelength λ reaches a maximum in Region III but a minimum in Region II at the low vertical position.

Furthermore, when $y \to 0$, the above feature is verified by a qualitative relationship:

$$\frac{C_5\left(e^{2\beta y}-1\right)}{C_3 e^{2\beta y}+C_4} < \frac{C_2}{C_1}\left(e^{2\beta y}-1\right) < 1. \tag{36}$$

This relationship indicates that under the following conditions in different regions, the same wavenumber β, the same streamwise position x, the same strength of streamwise vorticity whenever on or near the walls, and the same wall-normal height y ($< h$), then the increasing rate of the vertical vorticity or the inclined angle of the vortex lines along the x-direction is the greatest in Region III but the smallest in Region II.

3.6.3. Effect of ejections

Then, the central question of the key effect of the ejections or upward flow with $+|v|$ on the lifting-up mechanism or the increasing vertical vorticity naturally arises. The following four aspects should be carefully discussed. The first aspect is the vertical velocity distributed in each region (I, II and III). In the present physical model, the vertical velocity is assumed to be uniformly distributed along the x direction, regardless of whether it is located in Region I, II or III. This indicates that the lifting effect of $+|v|$ is also effective in each region, regardless of whether it is in the start or the end of each region. In other words, the quasistreamwise vortex should be lifted uniformly with the same uniform distribution of the vertical vorticity (i.e. , $\omega_y = 0$ without any inclination of vortex line), rather than the gradual increasing vertical vorticity predicted by the present model.

The second aspect is thus about the magnitude of the vertical velocity in each region (I, II and III). In the present analytical model, the intensity of the streamwise vorticity in each quasistreamwise vortex core is further assumed to be equal in each region without any viscous diffusion, which implies that the quasistreamwise vortex would induce the same magnitude of vertical velocity according to the Biot–Savart law. Then, the lifting mechanism, owing to a positive vertical velocity with the same magnitude, would lead to the exact same inclination of the vortex line in each region. However, the theoretical relationship, Eq. (36), suggests that the inclination angle is smaller in Region II but larger in Region III.

Then, the third aspect is the effect of the viscous forces, mainly dissipation and diffusion, on the already formed quasistreamwise vortex in each region. It is already known that viscous diffusion would reduce the vorticity in the present quasistreamwise vortex core transported downstream. As a result, the induced vertical velocity would also be weakened downstream. The lifting-up mechanism due to ejections with these weakened vertical velocities would cause the inclined angle of the quasistreamwise vortex to gradually decrease downstream. Therefore, the vortex lines in the two legs are possibly tilted downward. However, two legs are actually inclined increasingly or always upward, as shown in Fig. 2.

The fourth aspect, which is the distribution of the vertical velocity in the (y, z) plane, is discussed. As shown in Fig. 4(b) and Eq. (3a)(a), v is positive near the head at $z \sim \frac{1}{2}\lambda$ and negative at $z \sim 0$ and λ, but it is almost zero at $z \sim \frac{1}{4}\lambda$ and $\frac{3}{4}\lambda$ where two legs are located. This indicates that the effect of $+|v|$ is mainly on the lifting of the head, rather than the two legs or quasistreamwise vortices. In other words, if $+|v|$ at $z \sim \frac{1}{2}\lambda$ has

a lifting (ejection) effect on the two legs, then it is reasonably concluded that $-|v|$ at $z \sim 0$ and λ has a pressing-down (sweep) effect on the same legs. Consequently, both effects cancel each other out, and the two legs are always horizontal without any inclination.

In summary, it can be concluded that the lifting-up mechanism is not totally attributed to the ejections with a positive vertical velocity between the two legs. There must be a new mechanism under the sufficient consideration of these four aspects, unrelated to the magnitude of the positive vertical velocity varying along the x and z directions.

3.6.4. New mechanism: vortex-induced vortex

Finally, as indicated in the first sign law, the lifting mechanism is attributed to the vortex-induced vortex. In each region, whenever the quasistreamwise vortex is completely attached to the wall in Region I, or when it leaves the wall in Region II until in Region III, $\pm|\omega_y|$ are naturally induced by $\pm|\omega_x|$, respectively, mainly in the two legs or quasistreamwise vortices. This reveals the physical phenomenon that once the quasistreamwise vortex is close to and attached to the horizontal wall, the induced wall-normal vorticity causes the quasistreamwise vortex to have a natural tendency to leave far away from the wall, e.g. , if the viscous forces are strong enough with a high level of wall-normal vorticity, the quasistreamwise vortex enters into the outer region of the boundary layer. Such a lifting-up mechanism is theoretically unrelated to the magnitude of the quasistreamwise vortex and its variation and the induced positive vertical velocity in the ejections. Therefore, ejections could be regarded as the associated result of the already formed quasistreamwise vortex, as well as the positive vertical velocity. This lifting-up process typically undergoes a linear effect because of the linear viscous forces in the present dynamics Eq. (1), rather than a nonlinear effect owing to nonlinear inertial forces.

In addition, the relationship, Eq. (36), also presents an interesting property that possibly appears under certain parameters. The condition that $|\omega_x|$ is up to the maximum $A_{\omega_{x1}}$ at the wall in Region I is associated with the initial generation of two legs. Once the induced ω_y increases to a certain value, which leads to two legs lifting up slightly, $|\omega_x|$ then reduces down to $A_{\omega_{x2}}$ at the wall, as shown in Fig. 5(b), and the two legs evolve into Region II. Because the smallest ratio ω_y/ω_x is in Region II in Eq. (36), the induced ω_y increases very slowly. This results in the two legs stretching downstream over a longer distance (i.e. , $\lambda_{x2} > \lambda_{x1}$) until $|\omega_x|$ is zero at the wall in Region III. Thus, the two legs in Region II still appear to be horizontal, which is well consistent with the physical picture in Fig. 2(b). In Region III, these two slender legs are quickly slanted upward due to the greatest ratio ω_y/ω_x in Eq. (36). If this process occurs only in the viscous sublayer, the weak inertial forces have little contribution on the two slender legs through stretching. Therefore, this property is completely attributed to the viscous forces. Moreover, it is also expected that the slanted angle of the head in Region IV is determined by a kind of balance between the inertial forces and the viscous forces. Because the inertial forces intensify ω_x through streamwise stretching in the outer region with a higher mean velocity $U(y)$, while the viscous forces increase ω_y through the present mechanism of the vortex-induced vortex or the so-called vortex induction mechanism.

For the quasistreamwise vortices at high Reynolds numbers, the disappearance of the head-like structure could be attributed to following physical reasons. As shown in Fig. 13 only for Regions I and II, the induced vertical vorticity increases as the wall-normal distance increases in the viscous sublayer. However, at a high Reynolds number, the viscous sublayer is very thin and almost close to the wall, i.e. , $y \to 0$; therefore, the viscous forces are weak, and the vortex induction mechanism is greatly weakened, as the first reason. The stretching from the strong inertial forces, as the second reason, in the logarithmic layer leads to the increase in the streamwise vorticity. These coupling reasons cause the vertical vorticity to almost disappear at $y \to 0$, i.e. , $\omega_y \to 0$. However, as stated above in the first sign law, because the spanwise vorticity $\omega_z (\approx \Omega_z)$, which increases as the Reynolds number increases, near this quasistreamwise vortex is much larger than the amplitudes of ω_x and $\omega_y \sim 0$, it is impossible to show the isosurface or contour of ω in the head (assumed to exist) in both the experiments and simulations.

3.7. Physical meaning of the present hairpin vortex model

As reported in previous work [33], and considering the above analysis for both the vorticity sign laws and the associated lifting-up mechanism, the physical meaning in the present hairpin vortex model can be obtained as follows:

(i) The first sign law indicates that the inclined direction of the two legs or quasistreamwise vortices, mainly associated with the streamwise and vertical components of vorticity, is specific in the longitudinal plane, i.e. , the x–y plane.

(ii) The second sign law shows the specific rotational direction of the 3-D vortex in the hairpin paradigm, whenever it is in the upper or lower flat plate.

(iii) For the three components of vorticity, ω_x and ω_y are intrinsically dependent on each other. Only ω_z and Ω_z are mainly determined by the 2-D mean shear flow originally in the boundary layer, but $\delta\omega_z$ is a spanwise disturbing vorticity which causes ω_z or Ω_z to periodically increase and decrease across the span.

Furthermore, a physical feature provided by the theoretical model in Region I is discussed as follows. The streamwise vorticity in the two legs is assumed to be uniformly distributed along the streamwise direction in the three regions (I, II and III). Once the vertical vorticity increases to a certain intensity, the quasistreamwise vortex is gradually lifted away from the wall, e.g. , in Regions II and III. From Figs. 7(b) and 8(b), the vertical vorticity increases with increasing wall-normal distance y, as well as the streamwise vorticity. However, in Region I, as shown in Fig. 6(b), the streamwise vorticity with a maximum at the wall decreases with y because the quasistreamwise vortex is attached to the wall, i.e. , $y_{\omega_x \max} = 0$, while the vertical vorticity still increases away from the wall. This means that the induced vertical vorticity would reach its maximum at a certain height away from the wall, i.e. , $y_{\omega_y \max} > 0$, and would then dissipate due to the viscous forces. This is a new feature that mainly exists in Region I, which has two different heights for the maxima of the attached quasistreamwise vorticity and induced wall-normal vorticity, i.e. , $y_{\omega_x \max} \neq y_{\omega_y \max}$, although $|\omega_y|$ is still far less than $|\omega_x|$.

Based on the above feature in Region I, another physical meaning in this hairpin model is identified. The induced wall-normal vorticity is zero at the start $x = 0$ and increases downstream, as shown in Fig. 13(a); the induced spanwise vorticity $\delta\omega_z$ also increases downstream as shown in Fig. 6(b). In addition, the viscous diffusion through the normal gradient of the vorticity and dissipation all lead to the vorticity in the vortex decreasing, e.g. , the streamwise vorticity in the present quasistreamwise vortex. However, the introduced uniform quasistreamwise vorticity downstream is invariant in the present physical model. Consequently, the induced wall-normal vorticity obviously does not originate physically from either viscous effect. Thus, the vortex induction mechanism revealed by the present model is regarded as the third effect of the viscous forces on the spacial redistribution of the vorticity, referred to as viscous induction. Meanwhile, as reported in previous work [33] and from the viewpoint of the vorticity generation, such viscous induction is the indirect effect

of viscous forces, except viscous shearing near the wall as a direct effect.

Interestingly, this induction mechanism is hidden in the solutions satisfying the vortex dynamics governed by the Laplace's equation of disturbed vorticity, Eq. (2), coupled with the necessary and essential boundary condition of the solid wall. Physical reasons can be analyzed from the following several aspects in the present upper surface of the flat plate. The first is one limiting case with extremely high viscosity, so that there is $Re \to 0$, i.e. , the Stokes flow only governed by the Stokes equation, Eqs. (1) and (2). The main shear flow is always two-dimensional. Once the quasi-streamwise vorticity is introduced and the wall-normal vorticity is induced accordingly, these vorticities would be quickly died away due to high viscous diffusion and dissipation. As for the second aspect, another limiting case is the flow with extremely small viscosity, i.e. , $Re \to \infty$, approximately governed by the Euler's equation. Even if the wall-normal vorticity is induced, its magnitude is so small that the quasi-streamwise vortex still extends downstream without obvious inclination, as discussed before. Besides, the disturbance of inertial forces is the third aspect. The spatial distribution of vorticity is commonly and almost determined by coupling effects of inertial and viscous forces, such as convection, stretching and diffusion. The viscous induction only occurs in the local flow region where the viscous forces are dominant. Resultantly, it is hard to identify solutions of such induction from total velocity and vorticity fields obtained in experiments and numerical simulations. Howbeit, only vorticity sign laws indicate such local solutions of viscous induction. In other words, the vorticity sign laws, particularly the first sign law, and inclination of 3-D vortex in the longitudinal plane, actually originated from the local Stokes solutions, are illustrated as a kind of fluid dynamical behaviors dominated by the Navier–Stokes solutions, and are thus reasonably misunderstood as coupling effects of inertial and viscous forces.

Finally, the effect of the inertial forces, i.e. , convection along the (local) streamwise direction, is taken into account. The inertial forces can determine the spatial direction of the vorticity evolution, while the vorticity with a specific sign and sign relationship are presently determined by the viscous forces. Thus, for the above feature, i.e. , $y_{\omega_x \max} \neq y_{\omega_y \max}$, coupling effects of the convection and viscous induction result in an induced wall-normal vorticity with specific signs appearing in a certain downstream and wall-normal position. This indicates that coupling effects can be used to explain a kind of physical phenomenon, that is, the physical origin of the streamwise vorticity appearing in the shear layers and shedding vortices in a bluff body's wake. Two typical examples are the (pure) mode A in the 3-D laminar wake transition of a square-section cylinder at $Re = 180$ [44] and a circular-section cylinder at $Re = 200$ [36]. Among them, the vertical vorticity along the local flow region is attached on the cylinder's rear surface. Then, through the presence of viscous induction and coupling convection downstream, the streamwise vorticity with a specific sign is induced in the shear layers and then shed with the shedding spanwise vortex, as reported in these works [36,44].

3.8. Self-similarity of the disturbed vorticity only under the viscous effect

Only under the effect of viscous forces on the hairpin vortex, the self-similarity is theoretically revealed. From Eqs. (14a), (18a) and (22a), it seems that the disturbed vorticity $(\omega_x, \omega_y, \delta\omega_z)$ is correlated to the spanwise wavelength λ or wavenumber β. In fact, if we introduce the following spatial transformation as

$$x' = \beta x, \quad y' = \beta y, \quad z' = \beta z, \tag{37}$$

then we can obtain the following simplified vorticity fields in Region I,

$$\omega_x = -C_1 \mathrm{e}^{-y'} \sin z', \tag{38a}$$

$$\omega_y = -C_2 x' \left(\mathrm{e}^{y'} - \mathrm{e}^{-y'}\right) \sin z', \tag{38b}$$

$$\delta\omega_z = -C_2 x' \left(\mathrm{e}^{y'} + \mathrm{e}^{-y'}\right) \cos z', \tag{38c}$$

in Region II,

$$\omega_x = -\left(C_3 \mathrm{e}^{y'} + C_4 \mathrm{e}^{-y'}\right) \sin z', \tag{39a}$$

$$\omega_y = -C_5 x' \left(\mathrm{e}^{y'} - \mathrm{e}^{-y'}\right) \sin z', \tag{39b}$$

$$\delta\omega_z = -C_5 x' \left(\mathrm{e}^{y'} + \mathrm{e}^{-y'}\right) \cos z', \tag{39c}$$

and in Region III,

$$\omega_x = -C \left(\mathrm{e}^{y'} - \mathrm{e}^{-y'}\right) \sin z', \tag{40a}$$

$$\omega_y = -C x' \left(\mathrm{e}^{y'} - \mathrm{e}^{-y'}\right) \sin z', \tag{40b}$$

$$\delta\omega_z = -C x' \left(\mathrm{e}^{y'} + \mathrm{e}^{-y'}\right) \cos z'. \tag{40c}$$

The spacial distributions of such disturbed vorticity fields in the three regions are all unrelated to the wavelength λ or wavenumber β. Consequently, the disturbed vorticity in the whole hairpin vortex at any scale (only spanwise variation) is self-similar in the relative coordinate system (x', y', z') scaled by the wavelength only under the effect of viscous forces. This is referred to as the self-similarity of the disturbed vorticity in a single hairpin vortex.

3.9. Effect of boundary conditions in the basic assumption (A6)

Here, the effect of the basic assumption (A6) on the above qualitative analysis is discussed, where ω_y and $\delta\omega_z$ disappear at the start $x = 0$. Such an assumption is only physically reasonable in Region I, because the disturbed streamwise vorticity is initially generated due to turbulence. Once the hairpin vortex leg evolves in Region II, ω_y at $x = 0$ is affirmatively nonzero and equal to that at $x = \lambda_{x1}$ in Region I, as shown in Eq. (14a). A similar situation in Region III is also effective, correlated with Region II.

Therefore, at the end of Region I ($x = \lambda_{x1}$), we have:

$$\omega_y|_{\lambda_{x1}} = -C_2 \beta \lambda_{x1} \left(\mathrm{e}^{\beta y} - \mathrm{e}^{-\beta y}\right) \sin(\beta z), \tag{41a}$$

$$\delta\omega_z|_{\lambda_{x1}} = -C_2 \beta \lambda_{x1} \left(\mathrm{e}^{\beta y} + \mathrm{e}^{-\beta y}\right) \cos(\beta z). \tag{41b}$$

As an example, Eq. (8a) presents the following relationship at $x = 0$ in Region II,

$$\frac{\partial C_u}{\partial z} = \omega_y|_{\lambda_{x1}}, \quad \frac{\partial C_u}{\partial y} = -\delta\omega_z|_{\lambda_{x1}}. \tag{42}$$

Considering the non-slip boundary condition on the wall, the coefficient C_u is written as

$$C_u(y, z) = C_2 \lambda_{x1} \left(\mathrm{e}^{\beta y} - \mathrm{e}^{-\beta y}\right) \cos(\beta z), \tag{43}$$

and the disturbed streamwise velocity u is obtained as follows:

$$u(x, y, z) = x \left(\frac{\mathrm{d}A_v}{\mathrm{d}y} + \beta A_w\right) \cos(\beta z) + C_2 \lambda_{x1} \left(\mathrm{e}^{\beta y} - \mathrm{e}^{-\beta y}\right) \cos(\beta z). \tag{44}$$

It is found out that the appearance of nonzero C_u has no effect on the solution of the vorticity equation, Eq. (9a), due to $(\frac{\mathrm{d}^2}{\mathrm{d}y^2} - \beta^2)(\frac{\partial C_u}{\partial y}) = (\frac{\mathrm{d}^2}{\mathrm{d}y^2} - \beta^2)(\frac{\partial C_u}{\partial z}) \equiv 0$. Subsequently, it can be concluded that the two vorticity sign laws obtained above still prevail in Region II, as well as the third sign law because of the identical qualitative distribution of u and other features. Such a conclusion is also qualitatively valid in Region III.

4. Conclusions

In the present paper, the vorticity sign laws in a hairpin vortex are investigated in the viscous sublayer of a laminar boundary layer, i.e. , the immediate neighborhood of a solid wall. The hairpin vortex adopts the classical Theodorsen's hairpin paradigm [10] while taking numerical results into consideration. By means of the vortex-induced vortex theory first proposed by Lin et al. [31], originally used for external flow past a bluff body, the vortical structure in the present hairpin vortex is analyzed in the immediate neighborhood of a wall where the viscous forces are dominant and the inertial forces are ignored. Through the vorticity decomposition in the hairpin vortex, the focus is mainly on the disturbed vorticity field in the two legs or quasistreamwise vortices. Furthermore, the preliminary analysis of the streamwise vorticity at and near the wall provides different boundary conditions corresponding to different regions in the hairpin vortex, especially in Regions I, II and III. Finally, the disturbed vorticity fields, as well as the disturbed velocity and pressure, in three regions are obtained.

Based on the distribution of these disturbed vorticities, two vorticity sign laws are derived accordingly. Whether in Regions I, II or III, the first sign law reveals that the wall-normal vorticity with a specific sign is only induced by the wall-tangent vorticity in the quasistreamwise vortex, which is the central idea of the vortex-induced vortex theory. The second sign law indicates the specific sign combination of the three vorticity components in the whole vortical structure. Moreover, by comparing the vortices and their sign laws typically in an external flow past a bluff body and an internal flow through a pipe at low and laminar Reynolds numbers, the intrinsic relationship between these 3-D vortices and the hairpin vortex provides the same two sign laws and sign combinations for these vortical structures. These sign relationships may be regarded as the universal physical mechanism in the present external and internal flows because these laws are unrelated to the Reynolds number and disturbances (such as wavelength). The generalized Π-type vortex, as a category of a vortex in which the three components of the vorticity are consistent with both sign laws, is constructed based on the quadrant analysis in the $\omega_x - \omega_y$ plane.

In the disturbed velocity and pressure fields, the backward flow between two legs and the forward flow between two adjacent hairpin vortices are associated with ejections and sweeps. The disturbed pressure, or the actual frictional pressure loss, near the head gradually decreases downstream, but that near the outboard region increases downstream.

According to the special distribution of disturbed backward flow, the third sign law for the streamwise and vertical components of the disturbed velocity is obtained in Regions I, II and III. This further indicates that the specific sign of the Reynolds shear stress, $-\rho uv$, is always positive in Regions I, II and III, as the induced result of the streamwise vortex or vortex pair in the boundary layer.

However, a new mechanism used to explain the lifting of the hairpin vortex is proposed. Through careful analysis and discussion on the effects of ejections with positive wall-normal velocities proposed previously, it is concluded that the lifting-up mechanism cannot be completely attributed to ejections because ejections are closely dependent on the distribution of the wall-normal velocity. Then, according to the first sign law, it is determined that the mechanism of the vortex-induced vortex is also suitable for the lifting-up mechanism in the hairpin vortex. This lifting process is predominantly a linear effect of the viscous forces. Interestingly, this is the first time that it is theoretically discovered that the increasing rate of the ratio ω_y/ω_x, as well as that of the inclination angle, is the smallest in Region II but the largest in Region III under only the effect of viscous forces.

In the present theoretical model, the physical meaning of the vorticity sign laws mainly indicates that the direction of a vorticity vector in the present hairpin vortex is specific, as well as the inclined direction of the two legs. Based on the variations in the wall-normal and streamwise components of the vorticity in Region I, the vortex induction mechanism is identified as the third effect of the viscous forces, that is, the viscous induction. Viscous induction belongs to a kind of interaction between the vortex and wall, satisfying Laplace's equation for the disturbed vorticity. In summary, as for viscous forces, the viscous induction is not only the third effect on the vorticity redistribution, different from viscous diffusion and dissipation, but also the indirect effect on the vorticity generation, different from the viscous shearing near the wall.

Finally, through a transformation into the relative coordinate system scaled by the wavelength, the self-similarity of the disturbed vorticity in the hairpin vortex, that is, the transformed vorticity unrelated to the disturbance wavelength, is reported as a new feature under only the effect of viscous forces.

Declaration of competing interest

The authors declare that they have no known competing financial interests or personal relationships that could have appeared to influence the work reported in this paper.

References

[1] M.S. Acarlar, C.R. Smith, A study of hairpin vortices in a laminar boundary layer. Part 2. Hairpin vortices generated by fluid injection, J. Fluid Mech. 175 (1987) 43–83.
[2] H. Schlichting, Boundary Layer Theory, McGraw-Hall Book Company(seventh edition, 1979.
[3] M.R. Head, P. Bandyopadhyay, New aspects of turbulent boundary layer structure, J. Fluid Mech. 107 (1981) 297–338.
[4] S.J. Kline, W.D. Reynolds, F.A. Schraub, P.W. Runstadler, The structure of turbulent boundary layers, J. Fluid Mech. 30 (1967) 741–773.
[5] W. Schoppa, F. Hussain, Coherent structure generation in near-wall turbulence, J. Fluid Mech. 453 (2002) 57–108.
[6] J. Jiménez, G. Kawahara, M.P. Simens, M. Nagata, M. Shiba, Characterization of near-wall turbulence in terms of equilibrium and bursting solutions, Phys. Fluids 17 (2005) 015105.
[7] D. Swearingen, R.F. Blackwelder, The growth and breakdown of streamwise vortices in the presence of a wall, J. Fluid Mech. 182 (1987) 255–290.
[8] C.B. Lee, X.Y. Jiang, Flow structures in transitional and turbulent boundary layers, Phys. Fluids 31 (2019) 111301.
[9] A.A. Townsend, Equilibrium layers and wall turbulence, J. Fluid Mech. 11 (1961) 97–120.
[10] T. Theodorsen, Mechanism of turbulence, in: Second International Midwest Conference on Fluid Mechanics, Ohio State University, 1952, pp. 1–19.
[11] Y.S. Wang, W.X. Huang, C.X. Xu, On hairpin vortex generation from near-wall streamwise vortices, Acta Mech. Sinica 31 (2015) 139–152.
[12] J. Yoshikawa, Y. Nishio, S. Izawa, Y. Fukunishi, Key structure in laminar-turbulent transition of boundary layer with streaky structures, Theor. Appl. Mech. Lett. 9 (2019) 32–35.
[13] C.R. Smith, J.D.A. Walker, A.H. Haidari, U. Sobrun, On the dynamics of near-wall turbulence, Phil. Trans. R. Soc. A 336 (1991) 131–175.
[14] R.J. Adrian, C.D. Meinhart, C.D. Tomkins, Vortex organization in the outer region of the turbulent boundary boundary layer, J. Fluid Mech. 422 (2000) 1–54.
[15] S.C. Deng, C. Pan, J.J. Wang, G.S. He, On the spatial organization of hairpin packets in a turbulent boundary layer at low-to-moderate Reynolds number, J. Fluid Mech. 844 (2018) 635–668.
[16] Y.G. Guezennec, U. Piomelli, J. Kim, On the shape and dynamics of wall structures in turbulent channel flow, Phys. Fluids A 1 (1989) 764–766.
[17] M. Stanislas, L. Perret, J.M. Foucaut, Vortical structures in the turbulent boundary layer: A possible route to a universal representation, J. Fluid Mech. 602 (2008) 327–382.
[18] A. Schröder, R. Geisler, K. Staack, et al., Eulerian and Lagrangian views of a turbulent boundary layer flow using time-resolved tomographic PIV, Exp. Fluids 50 (2011) 1071–1091.
[19] A. Lozano-Durán, O. Flores, J. Jiménez, The three-dimensional structure of momentum transfer in turbulent channels, J. Fluid Mech. 694 (2012) 100–130.

[20] A. Lozano-Durán, J. Jiménez, Time-resolved evolution of coherent structures in turbulent channels: Characterization of eddies and cascades, J. Fluid Mech. 759 (2014) 432–471.
[21] S. Pirozzoli, M. Bernardini, Turbulence in supersonic boundary layers at moderate Reynolds number, J. Fluid Mech. 688 (2011) 120–168.
[22] P. Schlatter, Q. Li, R. Örlü, F. Hussain, D.S. Henningson, On the near-wall vortical structures at moderate Reynolds numbers, Eur. J. Mech. B/Fluids 48 (2014) 75–93.
[23] G. Eitel-Amor, R. Örlü, P. Schlatter, O. Flores, Hairpin vortices in turbulent boundary layers, Phys. Fluids 27 (2015) 025108.
[24] A. Shekar, M.D. Graham, Exact coherent states with hairpin-like vortex structure in channel flow, J. Fluid Mech. 849 (2018) 76–89.
[25] X. Wu, P. Moin, Direct numerical simulation of turbulence in a nominally zero-pressure-gradient flat-plate boundary layer, J. Fluid Mech. 630 (2009) 5–41.
[26] J. Jiménez, S. Hoyas, M.P. Simens, Y. Mizuno, Turbulent boundary layers and channels at moderate Reynolds numbers, J. Fluid Mech. 657 (2010) 335–360.
[27] A.E. Perry, S. Henbest, M.S. Chong, A theoretical and experimental study of wall turbulence, J. Fluid Mech. 165 (1986) 163–199.
[28] A.E. Perry, Marušić Ivan, A wall-wake model for the turbulence structure of boundary layers. Part 1. Extension of the attached eddy hypothesis, J. Fluid Mech. 298 (1995) 361–388.
[29] Marusic Ivan, On the role of large-scale structures in wall turbulence, Phys. Fluids 13 (2001) 735–743.
[30] R.J. Adrian, Hairpin vortex organization in wall turbulence, Phys. Fluids 19 (2007) 041301.
[31] L.M. Lin, S.Y. Shi, X.F. Zhong, Y.X. Wu, Mechanism of wavy vortex and sign laws in flow past a bluff body: vortex-induced vortex, Acta Mech. Sinica 35 (2019) 1–14.
[32] L.M. Lin, Vorticity sign law in three-dimensional wake of bluff body at low Reynolds number, Acta Phys. Sin. 69 (2020) 034701, (in Chinese).
[33] L.M. Lin, Y.X. Wu, Mechanism for vorticity in a secondary flow within a pipe: vortex-induced vortex, Phys. Fluids 32 (2020) 033602.
[34] L.M. Lin, Y.X. Wu, New interpretation of specific sign of Reynolds stress in the boundary layer on a flat plate, Theor. Appl. Mech. Lett. 8 (2018) 372–377.
[35] K.S. Yang, P.R. Spalart, J.H. Ferziger, Numerical studies of natural transition in a decelerating boundary layer, J. Fluid Mech. 240 (1992) 433–468.
[36] L.M. Lin, Z.R. Tan, DNS in evolution of vorticity and sign relationship in wake transition of a circular cylinder: (pure) mode A, Acta Mech. Sinica 35 (2019) 1131–1149.
[37] L.M. Lin, Wake Dynamics and Forces in the Flow Around the Square-Section Cylinder with a Geometric Disturbance, (PhD Dissertation), Institute of Mechanics, CAS, Beijing, China, 2007, (in chinese).
[38] L.M. Lin, S.Y. Shi, Y.X. Wu, Intrinsic relationship of vorticity between modes A and B in the wake of a bluff body, Theor. Appl. Mech. Lett. 8 (2018) 320–325.
[39] R.M. Darekar, S.J. Sherwin, Flow past a square-section cylinder with a wavy stagnation face, J. Fluid Mech. 426 (2001) 263–295.
[40] L.M. Lin, X.F. Zhong, Y.X. Wu, Acta Mech. Sinica 34 (2018) 812–829.
[41] Y.S. Kachanov, On a unierversal mechanism of turbulence production in wall shear flows, in: Recent Results in Laminar-Turbulent Transition, Vol. 86, in: Notes on numerical fluid mechanics and multidisciplinary design, 2004, pp. 1–12.
[42] M.K. Branden, S.E. Gregory, J.C. Dutton, Hairpin vortex structures in a supersonic, separated, longitudinal cylinder wake, Phys. Fluids 32 (2020) 046103.
[43] E.R. Corino, R.S. Brodkey, A visual investigation of the wall region in turbulent flow, J. Fluid Mech. 37 (1969) 1–30.
[44] L.M. Lin, S.Y. Shi, Y.X. Wu, Physical mechanism for origin of streamwise vortices in mode A of a square-section cylinder, Acta Mech. Sinica 35 (2019) 411–418.